PSC Optimization of 13.56-MHz Resistive Wireless Analog Passive Sensors

Babak Noroozi, *Member, IEEE*, and Bashir I. Morshed, *Member, IEEE*

(Invited Paper)

***Abstract*— Patient and health monitoring in real-life settings can be realized with passive, wireless, unobtrusive, and low-cost physiological signal monitoring. We have previously reported a new fully-passive sensor system, namely resistive wireless analog passive sensors (rWAPSs), based on inductive coupling for physiological signal collection. Fabrication of thin body-worn sensors using rWAPS technology requires planar printed spiral coils (PSC) as the inductive link. This paper describes a formal method to design and optimize this PSC coil for such a system and presents the results of a comparison of a commercial PSC and the optimal design developed with the proposed method. Iterative process is required to reach the optimal solution of this complex multivariate optimization problem. After optimum design based on given coil dimensions and track specifications, a coil pair with a two-layer PCB was fabricated. The secondary coil size was restricted to a small footprint of 20 mm, while the carrier frequency was selected as 13.56 MHz within ISM frequency band. Lower power consumption and higher sensitivity were set as the key criteria for the comparison of these designs. Experimental results confirm that although the sensitivity varies with respect to sensor resistance, the optimized design has a smaller footprint and offers a higher sensitivity in most sensor ranges, while consuming slightly less power. This proposed optimization approach of PSC design is practical for rWAPS and other similar inductively coupled sensors and can be utilized in body-worn, wearable, and implanted sensors.**

***Index Terms*— Body-worn sensors, fully passive sensors, impedance loading, inductive link, iterative optimization, printed spiral coil (PSC), wearable sensors.**

I. Introduction

Monitoring physiological signals in the regular life setting plays an important role in early and precision diagnostic and health tracking. Wireless wearable sensors as the general solution for continuous monitoring remove obtrusive wires, that are susceptible to noise and disconnection, making them more practical. A challenge for wireless wearable sensors is battery that makes them heavy, costly and requires maintenance. Hence, fully-passive wireless sensors that do not require battery at the sensor-side are suitable as body-worn sensors. We have previously presented [1], [2] a novel resistive wireless analog passive sensor (rWAPS) based on inductive coupling between sensor board and interrogator that employed printed spiral coils (PSCs) instead of the traditional solenoid coils that cannot be printed and has thicker profiles. Inductive coupling has been used extensively for power transmission in remote charging and implanted devices [3]–[12]. In order to have more comfortable wearing experience, they need to be flexible (thin profile), smaller (in size), and lightweight, and be sensitive over wide range of distances between sensor and interrogator coils. These coils occupy most of the floor plan of the sensor, hence, should be small in size with high sensitivity. However, these two factors usually have the reverse trend [1], [3], [5], [11] meaning that increasing sensitivity needs larger coil and decreasing the coil size weakens the mutual inductance that ends up to lesser sensitivity for the same amount of power consumption.

Even though radio frequency identification (RFID) and near-field communication (NFC) based sensor-tag are fully-passive and low cost, they are usually not optimal for physiological signal collection. These techniques utilize digital data encoding techniques for wireless link, which requires higher power compared to its counterpart of WAPS. Generally, in an RFID, power circuits and other low-power chips, consume energy that make them an unsuitable option for wearable sensors compared to WAPS [13], [14]. Moreover, resolution and sensitivity are still the bottlenecks of sensor-tag RFID [13], [15]. It should be noted that a typical RFID works once it is in reader's field and it requires power-up time that limits the sampling rate for high-frequency biopotentials like ECG [13], [14].

One implementation of WAPS relies on capacitive variation of a varactor that responds to bioelectric signals. Towe [16], [17], Baldwin *et al.* [18], Chae *et al.* [19]–[21], and Lekkala *et al.* [22] are among the pioneers to develop such capacitive WAPS (cWAPS). In those studies, an *LC* resonator with capacitive sensing (realized with a varactor) caused changes of the resonance frequency *fc* of the inductively coupled or backscattered signals. A surface acoustic wave chip has been used as a delay line for the modulated signals, thus differentiating backscattered signal from the interrogating signal [20], [23], [24].

In [22], ECG was recorded from 5 cm distance by two detecting methods: slope detector and phase locked reader. A major drawback of cWAPS sensing is that it is limited to voltage sensing only. Furthermore, the cWAPS approach

Manuscript received November 17, 2016; revised January 18, 2017 and January 30, 2017; accepted February 2, 2017. Date of publication March 2, 2017; date of current version September 1, 2017. This work was supported in part by the FedEx Institute of Technology Innovation under Grant 2013-537908 and in part by the National Science Foundation under Grant 1637250.

The authors are with the Department of Electrical and Computer Engineering, The University of Memphis, Memphis, TN 38152 USA (e-mail: bnoroozi@memphis.edu; bmorshed@memphis.edu).

Color versions of one or more of the figures in this paper are available online at http://ieeexplore.ieee.org.

Digital Object Identifier 10.1109/TMTT.2017.2666802

is based on frequency modulation (FM), as the resonant frequency (f_c) shifts due to the LC tank circuit. Thus, the interrogator requires a relatively larger bandwidth (BW) for each sensor and complex FM demodulator circuit must be implemented in the interrogator. Furthermore, very limited availability of capacitive transducer for various physical signals severely constrains its applicability.

In contrast, we have proposed an alternative technology, rWAPS, that is comprised of an RLC tank circuit where the inductor (L) and capacitor (C) determine the resonant frequency (f_c) for probing, while the load resistance (R) is a resistive transducer suitable for physiological signal measurement [1], [2], [25]. The working principle of rWAPS is based on the alteration of quality factor (Q) at the tuned frequency as the modality of measurement. The significant advantage of resistive transducer is that various physical signals can be measured with resistive transducers (such as light, pressure, and temperature) as well as bioelectric potentials can also be measured (with MOSFET as we have demonstrated earlier [2]). Furthermore, since the amplitude modulation (AM) operates in a narrower BW, the technique allows a larger number of sensors to be probed simultaneously within a given wireless BW and narrow BW (or high Q) increases the sensitivity [3], [4], [12]. Moreover, AM demodulators have less complexity compared to FM detectors. In addition, most of such resistive transducers are readily available as components off-the-shelf providing a large selection of low-cost physical signal measurement options.

We have previously presented a paper [26] that describes a method to optimize the PSC in order to have optimum inductive link in terms of smaller PSC size, higher sensitivity, and larger distance between coils. Within this scope of rWAPS, the PSC size, sensitivity, and power consumption for the same distance are the appropriate criteria for evaluating PSC designs. In [26], we presented the coil optimization procedure and the experimental results for probing biosignals. This paper extends these results in terms of comparing output sensitivities between a commercial PSC design and our optimized design.

Even though the coil design optimization research was conducted for some aspects like maximizing coupling coefficient (k) [9], maximizing the inductance density (Hennry/occupied area) [3], or strongly coupled regime [9], there are only a few works reported on coil optimization for maximizing the power efficiency [5], [11]. Furthermore, our previous report on rWAPS [1], [2] employed a coil design provided by Texas Instruments (TI) in [27, Sec. 6–8]. In this paper, we extend our work and present the comparison results of power consumption and sensitivity between an optimized PSC (based on an iterative algorithm) and a design provided by TI. We utilized various commonly used constraints for PCB fabrication, such as track width, space between tracks, and maximum coil size. The resultant optimal design was fabricated with dimensions of $w = 762$ μm (30 mil), $s = 508$ μm (20 mil), and coil area = 20 mm × 20 mm while the PSC designed by TI has dimensions of 50 mm × 38 mm (rectangular). The experimental results show better sensitivity and generally less power consumption for the optimal design.

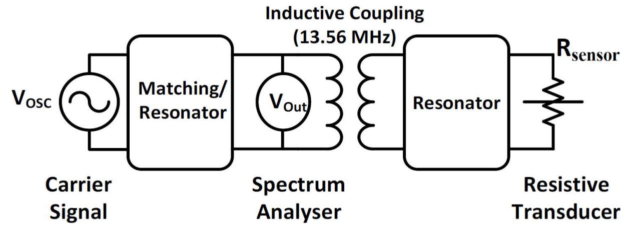

Fig. 1. Concept of rWAPS. Variation of resistive sensor changes the primary voltage proportional to mutual inductance.

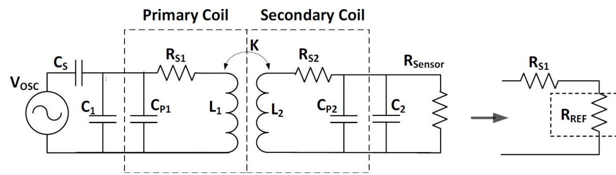

Fig. 2. Detail of rWAPS and the concept of reflected resistor (at the resonance frequency) from secondary to primary.

II. Hardware Concept

Fig. 1 shows the concept of rWAPS. The sensor side is fully-passive and includes the resistive sensor and secondary coil with a tuning capacitor, such that the secondary has the same resonance frequency as the primary. R_{sensor} is a resistive transducer that converts the physiological signal of interest to electrical resistances. The primary is excited with an input voltage at 13.56 MHz and transducer variation modulates the output voltage at the primary coil that is proportional to the sensitivity of the resistive sensor at the secondary coil.

The sensitivity depends on the distance between the coils, the power delivered by V_{OSC}, values of R_{sensor}, and the coil's specifications including self and mutual inductances and their quality factors. The goal of this paper is to have higher sensitivity with less delivered power. To achieve higher sensitivity with lower power, the efficiency from power source to R_{sensor} needs to be maximized.

A. Theory

Fig. 2 shows the schematic of rWAPS. C_{P1}, R_{S1}, L_1 and C_{P2}, R_{S2}, L_2 are the equivalent components for primary and secondary PSC, respectively. C_1 and C_2 are the tuning capacitors to adjust resonance frequencies on the desired values. C_S is the series matching capacitor between the primary coil and the signal generator (V_{OSC}). It can be shown [3], [5], [8] that the overall power efficiency (η) is dominated by

$$\eta = \frac{R_{\text{ref}}}{R_{\text{ref}} + R_{S1}} \times \frac{Q_{2L}}{Q_L} = \frac{k^2 Q_1 Q_{2L}}{1 + k^2 Q_1 Q_{2L}} \times \frac{Q_2}{Q_2 + Q_L} \tag{1}$$

where R_{ref} is the reflected resistor from secondary to primary side

$$R_{\text{ref}} = k^2 R_{S1} Q_1 Q_{2L} \tag{2}$$

k is the coupling factor between two coils, Q_1, Q_2, and Q_{2L} are the quality factors of primary, secondary without load, and secondary with load, respectively and they are calculated from the following equations [5]–[7], [28]:

$$Q_1 = \frac{L_1 \cdot \omega_0}{R_{S1}} \tag{3}$$

$$Q_2 = \frac{L_2 \cdot \omega_0}{R_{S2}} \quad \text{(Quality factor without load)} \tag{4}$$

$$Q_L = \frac{R_L}{L_2 \cdot \omega_0} \times \frac{1}{\left(\frac{1}{Q^2}+1\right)} \cong \frac{R_L}{L_2 \cdot \omega_0} \tag{5}$$

$$Q_{2L} = \frac{Q_2}{Q_2 + Q_L} \quad \text{(Quality factor with load).} \tag{6}$$

Equations (1)–(6) calculate the power efficiency based on the circuit with equivalent components of primary and secondary coils. Equivalent self-inductance (L) and parasitic resistor (R) and capacitor (C) can be calculated from the coil's physical characteristics with the following equations [3], [5], [11], [29]:

$$L = \frac{1.27 n^2 \mu_0 (d_o + d_i)}{4}\left[\ln\left(\frac{2.07}{\varphi}\right) + 0.18\varphi + 0.13\varphi^2\right] \tag{7}$$

$$R_S = \rho \frac{l_c}{w \cdot t} \times \frac{t}{\delta \cdot (1 - \exp(-t_c/\delta))} \tag{8}$$

$$\delta = \sqrt{\rho / \pi \mu f} \quad \text{(Skin effect).} \tag{9}$$

Conductor length and parasitic capacitor are given by

$$L_C = 4nd_O - 3nw - (2n-1)^2(s+w) \tag{10}$$

$$C_P = C_{PC} + C_{PS} \approx (\alpha\varepsilon_{rc} + \beta\varepsilon_{rs})\varepsilon_0 \frac{t_C}{S} l_g. \tag{11}$$

Gap length (between tracks) is given by

$$L_g = 4(d_O - nw)(n-1) - 4n(n+1)s \tag{12}$$

φ in (7) is called "fill-factor" and is defined as

$$\varphi = \frac{d_O - d_i}{d_O + d_i}. \tag{13}$$

Regarding (1)–(6), power efficiency increases with quality factors, and having larger quality factor requires smaller coil resistance and larger self-inductance that have opposite trends: increasing "L" increases "R" as well, unless we increase the track width (w) that ends in larger coil size. Therefore, for the specific input constraints for maximum coil dimension (d_O) and minimum space between tracks (s), there is a tradeoff between parameters. We attempt to find the best values that lead to maximum efficiency through an iterative method that has been provided in [5] to find the optimum values based on given constraints.

B. Input Constraints

Fig. 3 illustrates the coil parameters. There are some constraints that are defined by the device application and PCB manufacturer. The minimum limit for the space between tracks (s), track width (w) and track thickness are defined as 152.5 μm (6 mil), 152.5 μm, and 28.35 gr (1 oz that is equal to 1.5 mil), respectively, by the PCB manufacturer.

Another important constraint is the coil size that is restricted by the device application. We limit the maximum coil size to 40 mm for primary ($d_{O1\max}$) and 20 mm for the secondary ($d_{O2\max}$). Table I shows the applied constraints.

TABLE I

SPECIFIC PSC DESIGN CONSTRAINTS (1 mil = 25.4 μm)

Symbol	Parameter	Min	Max	Comment
w	Track width	6 mil	-	PCB manufacturer constraint
s	Track space	6 mil	-	PCB manufacturer constraint
d_{O1}	Primary Coil	-	40 mm	Application constraint
d_{O2}	Secondary Coil	20 mm		Application constraint
d_i	Coil Inner size	-	-	In some applications, it is limited

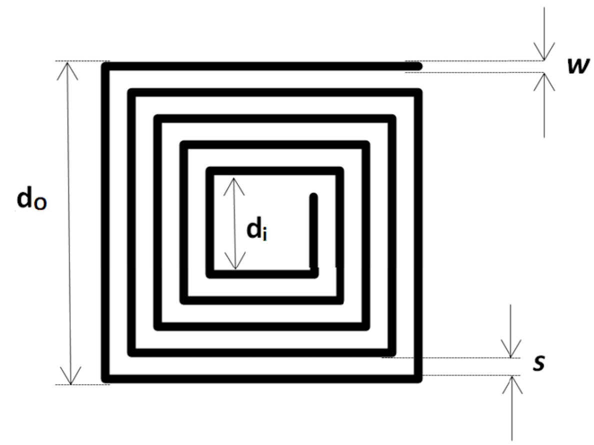

Fig. 3. Coil parameters and configuration.

III. COIL DESIGN

A. Iterative Method for Coil Optimization

Designing an optimized coil pair is a multivariable optimization problem. Among different methods, e.g., "genetic algorithm" or "particle swarm optimization," a well-established method [5], which reflects the effect of two optimized variables on the other variables through an iterative method, has been employed for this optimization process. In other words, the optimum values that maximize the power efficiency in each step have effect on the other steps that have to be iteratively performed until having less than 1% (residual error) improvement in efficiency. Fig. 4 shows the flowchart of the optimization algorithm.

B. Efficiency Behavior With Coil Parameters

To characterize the behavior of the efficiency with coil design parameters, the efficiency was analyzed over three inputs pairs as shown in Figs. 5–7. These figures show the efficiency behavior based on (1)–(13) versus two parameters while the other parameters are constant, as given in each figure. As it can be seen from Figs. 5–7, η is always increasing with respect to w_1, d_{O1}, and φ_1 but has a maximum with respect to w_2 and φ_1.

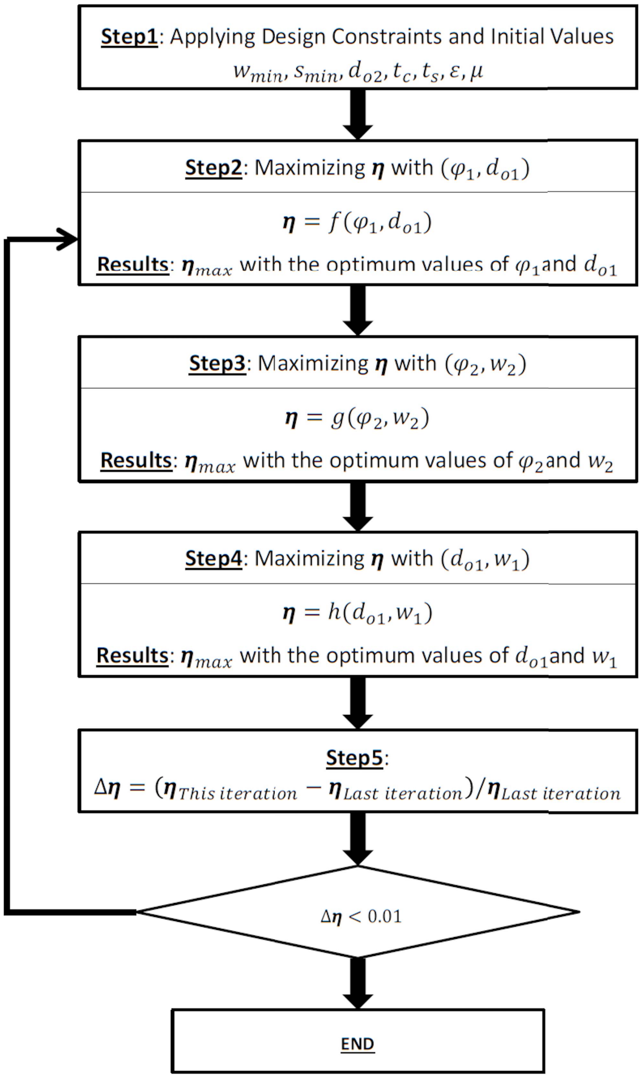

Fig. 4. Flowchart of the iterative optimization method.

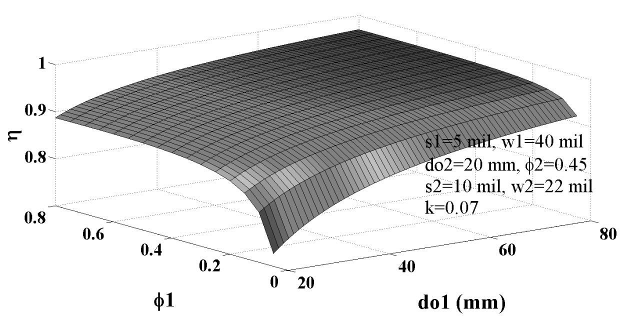

Fig. 5. Simulation results of the effect of primary fill-factor ($\boldsymbol{\varphi_1}$) and primary outer size ($\boldsymbol{d_{O1}}$) on the efficiency (η) (1 mil = 25.4 μm).

C. Coil Fabrication

The general parameters for the coil design have been listed in Table II. Some of the parameters are the PCB characteristics, and (α, β) are empirical parameters [5]. Several coil pairs, based on different constraints, have been designed and fabricated and their specifications are listed in Table III. L, R_S, and C_P in Table III are the coil equivalent components

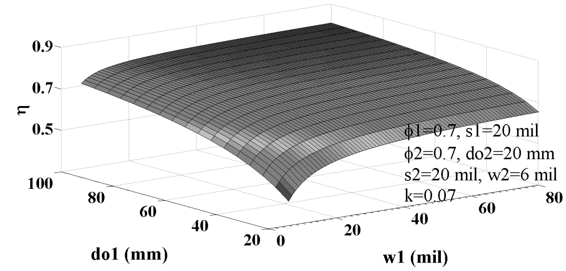

Fig. 6. Simulation results of the behavior of efficiency (η) with primary outer size ($\boldsymbol{d_{O1}}$) and primary track width ($\boldsymbol{w_1}$) (1 mil = 25.4 μm).

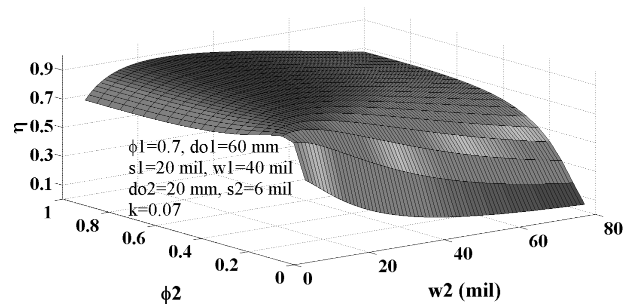

Fig. 7. Simulation results of efficiency (η) versus secondary track width ($\boldsymbol{w_2}$) and secondary fill-factor ($\boldsymbol{\varphi_2}$) (1 mil = 25.4 μm).

TABLE II
INPUT CHARACTERISTICS OF PSC DESIGN

Parameter		Symbol	Design Value
Conductor Thickness		t_c	38.1* µm
Conductor Material Properties		ρ, μ_{rc}	1.7×10^{-8}, 1
Substrate Thickness		t_s	1.6 mm
Relative Dielectric Constant	Substrate (FR4)	ε_{rs}	4.4
	Coating (Air)	ε_{rc}	1
Empirical coefficient [1]		(α, β)	(0.9,0.1)
Nominal Sensor resistance		R_{sensor}	1 kΩ
Coils separation distance		D	40 mm
Carrier frequency		f	13.56 MHz
Coupling factor		k	0.07

*: Referring to PCB manufacturer, the conductor thickness is 1 oz that is equal to 1.5 mil (38.1 µm) [http://OshPark.com].

corresponding to Fig. 2. Last column of Table III shows C_1 and C_2, which are the capacitors to tune the primary and secondary to the same resonance frequencies. For the larger values of C_1 and C_2, the primary and secondary resonance frequencies are less sensitive to the parasitic capacitors. The coils coupling factor (k) is considered as a constant value of 0.07 which is reasonable for such setup [4], [5], [28], [30]. The optimization process starts with specific s, d_{O2}, $d_{O1-\max}$, $w_{1,2-\min}$, and $w_{1,2}-\max$ as the constraints and ends with φ_1, φ_2, d_{O1}, and $w_{1,2}$. In Table II, n is the number of turns in the primary and secondary that depends on d_O, di, w, and s with the following equation:

$$n = \frac{d_O - d_i}{(s+w)} = \frac{d_o}{(s+w)} \times \frac{\varphi}{1+\varphi}. \tag{14}$$

All four designs in Table III, have been optimized for one extremum feature to see the maximum effect of that specific

TABLE III
FOUR OPTIMUM DESIGNS WITH DIFFERENT INPUT CONSTRAINTS (P: PRIMARY COIL, S: SECONDARY COIL, 1 mil = 2.54 μm)

	L (μH)	R_S (Ω)	C_P (pF)	d_O (mm)	d_i (mm)	w (mil)	s (mil)	n	Q	η	C (pF)
Design1											
P	8.2	3.6	7.5	40	7.3	20	15	19	227	0.80	9.3
S	0.7	0.6	1.1	20	11	20	15	6	103		207
Design2											
P	10.7	2.4	10.5	59	10.4	40	15	17.4	373	0.85	2.4
S	1.1	0.9	1.75	20	3.5	19	15	9.5	102		123
Design3											
P	2.0	0.76	0.65	40	7.1	50	20	9	228	0.85	68.2
S	1	0.65	1	20	3.5	31	6	9	133		133
Design4											
P	2	0.76	2.8	40	7.9	50	20	9	228	0.71	65
S	1.1	2.3	3.5	10	1.8	6	6	13.5	40		123

TABLE IV
SPECIFICATIONS OF TI COIL (P: PRIMARY COIL, S: SECONDARY COIL, 1 mil = 25.4 μm)

	L (μH)	R_S (Ω)	C_P (pF)	d_O (mm)	d_i (mm)	w (mil)	s (mil)	n	Q	η	C (pF)
Texas Instrument											
P	0.74	0.5	1	50×38	37×28	30	70	3	126	0.8	185
S	0.74	0.5	1	50×38	37×28	30	70	3	126		185

feature. Design1 has the largest primary turns, Design2 has the largest d_{O1}, Design3 has the widest w_1, and Design4 has the smallest d_{O2}. Design3, with the highest efficiency, has been selected for this paper to compare with the TI provided coil design.

As explained before, the larger C_1 and C_2 values make the primary and secondary resonance frequencies less sensitive to the parasitic capacitors and regarding this feature in Table III, again Design3 is preferred.

Table IV shows the suggested coil by TI (referred as Design0 here) [2], [27]. Theoretically, Design3 is optimized by the size and power efficiency. The different footprints of Design0 and Design3 can be compared in Fig. 8.

IV. RESULTS

A. Test Setup

After designing and fabricating Design0 and Design3, their equivalent circuits were measured with an *LCR* Analyzer (Agilent 4294A, 40 Hz–110 MHz). The axial separation between primary and secondary coils for all measurements was 40 mm. The measurement setup is shown in Fig. 9. The input voltage is applied by a function generator (RIGOL DG1022) through a coaxial cable via an SMA connector and the output is observed with a Spectrum

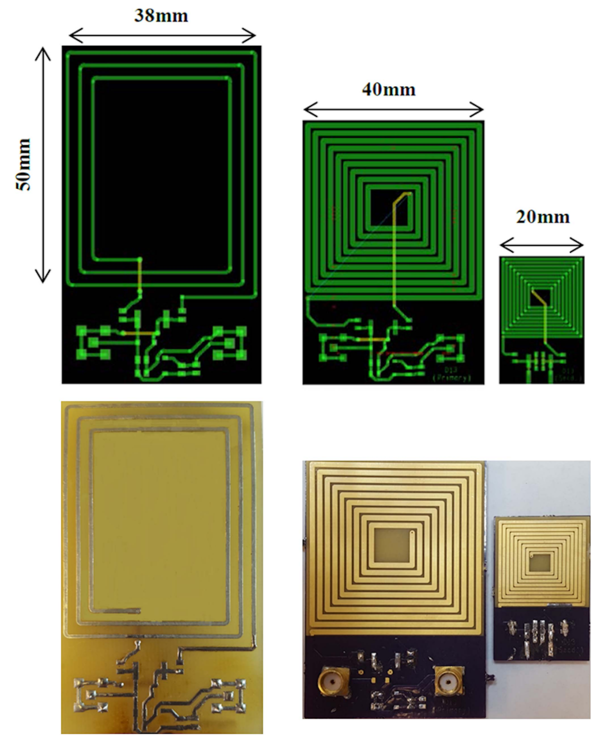

Fig. 8. (a) PCB layouts and (b) fabricated PCBs of Design0 and Design3. Design0 (TI design) has the same size of primary and secondary (left figure), while the optimized coil (Design3) has a smaller secondary (Primary coil in the middle, and secondary coil in the right).

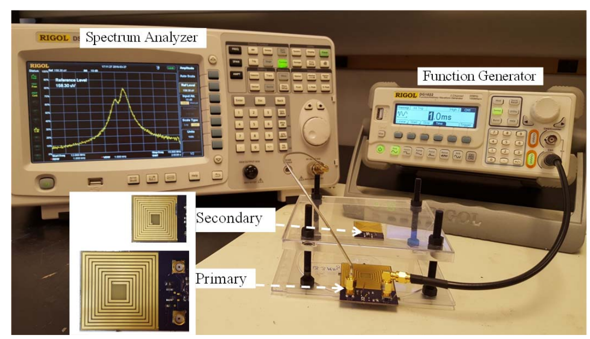

Fig. 9. Measurement setup. V_{osc} is applied by function generator and the output is observed with spectrum analyzer and oscilloscope. The distance between primary and secondary coils has been kept at 40 mm for all tests. (Inset: The photographs of the primary and the secondary PCBs are shown.)

Analyzer (RIGOL DSA 1030) and an Oscilloscope (Tektronix TDS 1001B). The circuit schematic for both Design0 and Design3 have the same configurations as shown in Fig. 10. In this figure, R_S is the internal resistor of signal generator, and C_S is the coupling capacitor for impedance matching. R_{sensor} at the secondary side is the resistive transducer whose variation reflects to V_{out} at the primary side.

B. Measurement Results

To compare Design3 with Design0, we define the sensitivity as follows:

$$\text{Sensitivity} = \frac{\Delta V_{\text{OUT}}}{\Delta R_{\text{Sensor}}}. \tag{15}$$

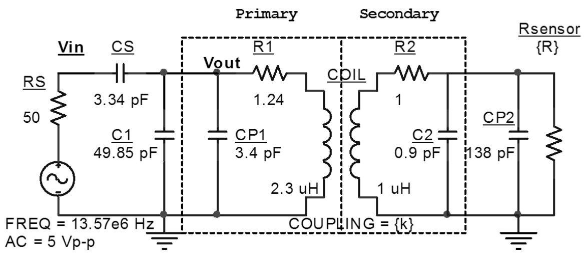

Fig. 10. Circuit under test with real measured values with an *LCR* analyzer for Design3. Design0 has the similar configuration with: $Cs = 3.9$ pF, $C_1 = 240$ pF, $C_{P1} = 1$ pF, $R_1 = 0.5\ \Omega$, $L_1 = 735$ nH and same values for the secondary.

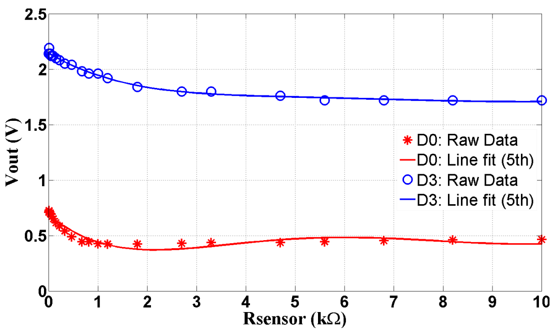

Fig. 11. Measurement results of the output voltage versus R_{sensor} for Design0 and Design3. Design3 has better response to R_{aensor} with respect to Design0.

To measure sensitivity with (15), R_{sensor} is changed from 0 Ω (short circuit) to 15 kΩ while V_{OSC} (without load) is 10 Vp-p. The sensitivity is too low to be considered for R_S more than 15 kΩ because the equivalent parallel resistor of the secondary coil and its tuning capacitor in the resonance frequency is as follows [31].

For Design0 ($R_2 = 0.5\ \Omega$, $L_2 = 735$ nH, $f = 12.25$ MHz)

$$R_{\text{eq}} = (1 + Q^2)R_{S2} = \left(1 + \left(\frac{L\omega}{R_2}\right)^2\right)R_2 = 6.4\ \text{k}\Omega. \quad (16)$$

For Design3 ($R_2 = 1\ \Omega$, $L_1 = 1\ \mu$H, $f = 13.23$ MHz)

$$R_{\text{eq}} = (1 + Q^2)R_{S2} = \left(1 + \left(\frac{L\omega}{R_2}\right)^2\right)R_2 = 6.9\ \text{k}\Omega. \quad (17)$$

Fig. 11 shows the Design0 and Design3 output voltages for comparison. According to Fig. 11, Design3 has approximately three times higher output voltage compared to Design0, which increases SNR and makes it more practical in the actual setting. Fig. 12 shows the sensitivity [defined by (15)], which is the derivative of V_{out} in Fig. 11. Regarding Fig. 12, sensitivity of Design0 and Design3 can be divided into four zones for R_{sensor} ranging between 0 and 8.2 kΩ. The sign of $(\Delta V_{\text{OUT}}/\Delta R_{\text{sensor}})$ reflects that the changes of V_{out} and R_{sensor} are in the same direction (positive sign) or the opposite direction (negative sign). Therefore, the sign is not important in comparing the sensitivities.

In the first zone, $R_{\text{sensor}} = 0$ to 570 Ω, Design3 has less sensitivity than Design0, namely the average sensitivity for Design0 is −31 and for Design3 is −19. In the second zone, $R_{\text{sensor}} = 570$ to 5.6 kΩ, the average sensitivity for

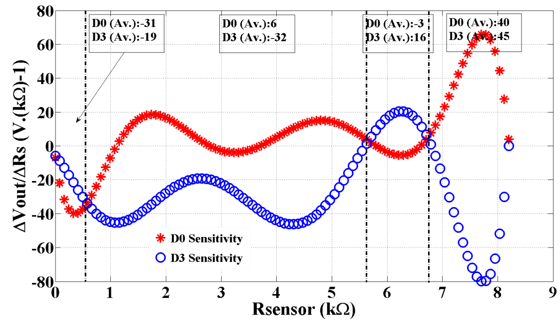

Fig. 12. Measurement results of the sensitivities for Design0 and Design3 with different R_{sensor}. There are four different zones by which the average sensitivities for both designs are mentioned in the plot.

Design0 and Design3 is 6 and 32, respectively. In the third zone, $R_{\text{sensor}} = 5.6$ kΩ to 6.7 kΩ, the average sensitivity of Design3 is again more than Design0, 3 for Design0 and 16 for Design3. In the fourth zone, $R_{\text{sensor}} = 6.7$ to 8.2 kΩ, the average sensitivity of Design0 is 40 and for Design3 is 45, which means that Design3 is again more sensitive.

Generally, when a sensor is driven with more power, the response is expected to be higher. Thus, in comparing the two coil designs in rWAPS, the amount of the power delivered by the signal generator needs to be considered and the sensitivity defined by (15) should be normalized with the delivered power. Delivered power is calculated by, first, measuring V_{in} and V_{out} (Fig. 10), and then, using the following equations:

$$I_S = \frac{V_{\text{in}} - V_{\text{out}}}{1/j\omega C_S} \quad (18)$$

$$P = I_S \times V_{\text{in}} \quad (19)$$

$$P_{\text{av}} = \int P dt. \quad (20)$$

According to (18)–(20), by changing R_{sensor} from zero to 8.2 kΩ and measuring V_{out} and V_{in}, P_{av} was calculated and is drawn in Fig. 13. Regarding Fig. 13, there is no significant difference between the two designs in terms of delivered power. In Fig. 13, the average delivered power can be split into two zones, by which in the left one ($R_{\text{sensor}} = 0\ \Omega$ to $R_{\text{sensor}} = 2.8$ kΩ), Design3 consumes 50 μW (2.5%) more power than Design0 and in the right zone ($R_{\text{sensor}} =$ 2.8–8.2 kΩ), Design3 consumes 20 μW (1%) less power than Design0. Thus, there is no significant difference between the two designs in terms of power consumption.

Fig. 14 shows the sensitivity that is normalized with delivered power. Regarding Fig. 14, normalized sensitivity can be split into four regions, by which in three regions Design3 has higher sensitivity than Design0.

V. Discussion

Since the iterative method calculated the coils' specifications based on maximum power efficiency, having higher normalized sensitivity with almost the same power in Design3 compared to Design0 was predictable. Even comparing the two designs in terms of sensitivity (not normalized) (Fig. 12) verifies that the new design (Design3) has higher sensitivity in most regions, regardless of power consumption. It can be

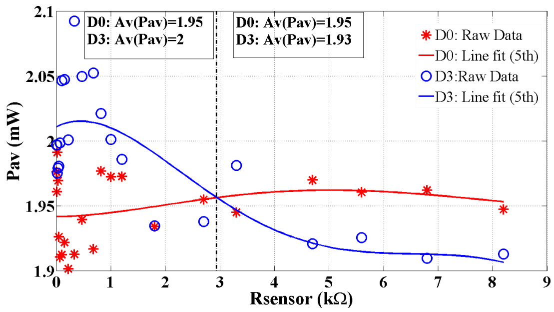

Fig. 13. Measurement results of the power consumption for Design0 and Design3. There are two zones at the two sides of 2.8 kΩ: on the left side Design3 has 50 μW more power consumption and in the right zone Design3 has 20 μW less power consumption on average.

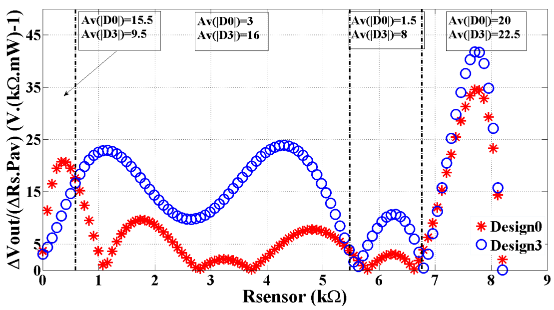

Fig. 14. Measurement results of the sensitivities of Design0 and Design3 as normalized with power consumption. There are four zones by which only for the leftmost zone, Design0 shows higher sensitivity while in the other zones Design3 is more sensitive than Design0.

explained in the way that if the coil design has been optimized for highest power transfer from primary to the secondary, it has been optimized for highest reflected or backscattered signal from secondary to the primary, as well.

According to Fig. 12, there are some variations in the sensitivity with R_{sensor} for both designs. It is worth to investigate in the future work, but it might be the effect of R_{sensor} on the coupling factor (k), quality factor, and the resonance frequency. Regarding the input parameters for coil optimization in Table II, the coil pair has been optimized for $R_{\text{sensor}} = 1$ kΩ, and it is seen from Fig. 12, that one of the maximum sensitivities of Design3 happens in this resistance, but changing R_{sensor} affects the other parameters and changes the sensitivity. In this paper, the coil has been optimized for specific R_{sensor} (1 kΩ) and consequently, for the specific quality factor, coupling factor, and resonance frequency that regarding Fig. 14, the result verifies the optimization. It is expected that a better result or higher sensitivity can be achieved by performing the optimization process for different values of R_{sensor} and its associated parameters and then choosing the region of R_{sensor} in which the sensitivity is maximized. The optimization in this paper has been performed for 13.56 MHz resonance frequency. However, since the frequency affects the impedance and quality factor, the optimization algorithm will lead to different coil specifications at other resonance frequencies.

VI. Conclusion

We have utilized an optimization algorithm that uses given constraints (size and fabrication) to design an optimum PSC. The optimum PSC has been designed within specifications (width and space of tracks, number of turns in primary and secondary coils and the primary size) to achieve the best power efficiency from carrier signal generator to the transducer. We also fabricated several coil pairs with different size constraints based on an iterative optimization method to have the best sensitivity of the output voltage to the resistive transducer. The best design in the sense of size and power efficiency has been tested, and compared to the standard coil pair provided by TI in terms of power consumption and sensitivity. While the optimized coil has less than half size (secondary) of the TI coil, it shows better sensitivity and almost the same power consumption.

In this paper, we have measured the best sensitive region (of R_{sensor}) for each design that should be considered in the application of rWAPS. The proposed coil design optimization will enable design of efficient fully-passive sensors that operate on inductive loading principle such as rWAPS. Such fully-passive sensors can have practical applications in wearable sensors for unobtrusive monitoring of patients for physiological signals at home and during routine daily activities. As rWAPS requires only a few inexpensive components, wearable sensors based on rWAPS can further be fabricated using flexible substrates that make them more comfortable, lighter, low cost, and disposable. On the other hand, flexible coils are subject to bending and it will change the coupling factor and efficiency. Future work will investigate the effect of bending on sensitivity that has impact on wearable and body-worn sensors development.

References

[1] S. Consul-Pacareu, D. Arellano, and B. I. Morshed, "Body-worn fully-passive wireless analog sensors for physiological signal capture through load modulation using resistive transducers," in *Proc. IEEE Healthcare Innov. Conf. (HIC)*, Oct. 2014, pp. 67–70.

[2] S. Consul-Pacareu, D. Arellano, and B. I. Morshed, "Body-worn fully-passive wireless analog sensors for biopotential measurement through load modulation," in *Proc. IEEE Biowireless Conf.*, San Diego, CA, USA, Jan. 2015, pp. 1–3.

[3] A. B. Islam, S. K. Islam, and F. S. Tulip, "Design and optimization of printed circuit board inductors for wireless power transfer system," *Circuits Syst.*, vol. 4, no. 2, pp. 237–244, 2013.

[4] R. Bashirullah, "Wireless implants," *IEEE Microw. Mag.*, vol. 11, no. 7, pp. S14–S23, Dec. 2010.

[5] U. Jow and M. Ghovanloo, "Design and optimization of printed spiral coils for efficient transcutaneous inductive power transmission," *IEEE Trans. Biomed. Circuits Syst.*, vol. 1, no. 3, pp. 193–202, Sep. 2007.

[6] U. Jow and M. Ghovanloo, "Modeling and optimization of printed spiral coils in air, saline, and muscle tissue environments," *IEEE Trans. Biomed. Circuits Syst.*, vol. 3, no. 5, pp. 339–347, Oct. 2009.

[7] M. Kiani, U. Jow, and M. Ghovanloo, "Design and optimization of a 3-coil inductive link for efficient wireless power transmission," *IEEE Trans. Biomed. Circuits Syst.*, vol. 5, no. 6, pp. 591–599, Dec. 2011.

[8] C.-S. Wang, G. A. Covic, and O. H. Stielau, "Power transfer capability and bifurcation phenomena of loosely coupled inductive power transfer systems," *IEEE Trans. Ind. Electron.*, vol. 51, no. 1, pp. 148–157, Feb. 2004.

[9] S. Konno, T. Yamamoto, and K. Koshiji, "Improvement of coupling coefficient by designing a spiral pattern formed on a printed circuit board," in *Proc. IEEE Wireless Power Transf. (WPT)*, May 2013, pp. 167–170.

[10] A. Kurs, A. Karalis, R. Moffatt, J. D. Joannopoulos, P. Fisher, and M. Soljačić, "Wireless power transfer via strongly coupled magnetic resonances," *Science*, vol. 317, no. 5834, pp. 83–86, 2007.

[11] F. Jolani, Y. Yu, and Z. Chen, "A planar magnetically coupled resonant wireless power transfer system using printed spiral coils," *IEEE Antennas Wireless Propag. Lett.*, vol. 13, pp. 1648–1651, 2014.

[12] V. Talla, V. Ranganathan, B. Mahoney, and J. R. Smith, "Dual band wireless power and bi-directional data link for implanted devices in 65 nm CMOS," in *Proc. ACM Workshop Med. Commun. Syst.*, New York, NY, USA, Aug. 2012, pp. 1–6.
[13] C. Occhiuzzi, S. Caizzone, and G. Marrocco, "Passive UHF RFID antennas for sensing applications: Principles, methods, and classifications," *IEEE Antennas Propag. Mag.*, vol. 55, no. 6, pp. 14–34, Dec. 2013.
[14] D. J. Yeager, P. S. Powledge, R. Prasad, D. Wetherall, and J. R. Smith, "Wirelessly-charged UHF tags for sensor data collection," in *Proc. IEEE Int. Conf. RFID*, Las Vegas, NV, USA, Apr. 2008, pp. 320–327.
[15] P. V. Nikitin and K. V. S. Rao, "Theory and measurement of backscattering from RFID tags," *IEEE Antennas Propag. Mag.*, vol. 48, no. 6, pp. 212–218, Dec. 2006.
[16] B. C. Towe, "Passive backscatter biotelemetry for neural interfacing," in *Proc. IEEE/EMBS Conf. Neural Eng.*, Kohala Coast, HI, USA, May 2007, pp. 144–147.
[17] B. C. Towe, "Systems and methods for wireless transmission of biopotentials," U.S. Patent 0 198 039, Aug. 5, 2010.
[18] H. A. Baldwin, S. W. Depp, A. R. Koelle, and R. W. Freyman, "Interrogation, and detection system," U.S. Patent 4 075 632, Feb. 21, 1978.
[19] H. N. Schwerdt *et al.*, "A fully-pasive wireless microsystem for recording of neuropotentials using RF backscattering methods," *J. Microelectromech. Syst.*, vol. 20, no. 5, pp. 1119–1130, 2011.
[20] H. N. Schwerdt, F. A. Miranda, and J. Chae, "Analysis of electromagnetic fields induced in operation of a wireless fully passive backscattering neurorecording microsystem in emulated human head tissue," *IEEE Trans. Microw. Theory Techn.*, vol. 61, no. 5, pp. 2170–2176, May 2013.
[21] H. N. Schwerdt, J. Chae, and F. A. Miranda, "Wireless performance of a fully passive neurorecording microsystem embedded in dispersive human head phantom," in *Proc. IEEE Antennas Propag. Soc. Int. Symp.*, Chicago, IL, USA, Jul. 2012, pp. 1–2.
[22] J. Riistama, E. Aittokallio, J. Verho, and J. Lekkala, "Totally passive wireless biopotential measurement sensor by utilizing inductively coupled resonance circuits," *Sens. Actuators A, Phys.*, vol. 157, no. 2, pp. 313–321, 2010.
[23] W. Luo *et al.*, "An integrated passive impedance-loaded SAW sensor," *Sens. Actuators B, Chem.*, vol. 187, pp. 215–220, Oct. 2013.
[24] A. Karilainen, T. Finnberg, T. Uelzen, K. Dembowski, and J. Müller, "Mobile patient monitoring based on impedance-loaded SAW-sensors," *IEEE Trans. Ultrason., Ferroelect., Freq. Control*, vol. 51, no. 11, pp. 1464–1469, Nov. 2004.
[25] B. I. Morshed, "Dual coil for remote probing of signals using resistive wireless analog passive sensors (rWAPS)," in *Proc. United States Nat. Commit. URSI Nat. Radio Sci. Meeting (USNC–URSI NRSM)*, Boulder, CO, USA, Jan. 2016, pp. 1–2.
[26] B. Noroozi and B. I. Morshed, "Formal method for PSC design optimization of 13.56 MHz resistive wireless analog passive sensors (rWAPS)," in *Proc. IEEE Radio Wireless Week Conf.*, Austin, TX, USA, Jan. 2016, pp. 8–11.
[27] J. A. Goulbourne, "HF antenna cookbook," Texas Instrum. Incorporated, Dallas, TX, USA, Tech. Rep. Lit. No. 11-08-26-001, 2004.
[28] K. Finkenzeller, *The RFID Handbook*. Hoboken, NJ, USA: Wiley, 2003.
[29] A. Eroglu, "Planar inductor design for high power applications," *Prog. Electromagn. Res. B*, vol. 35, no. 35, pp. 53–67, 2011.
[30] S. Raju, R. Wu, M. Chan, and C. P. Yue, "Modeling of mutual coupling between planar inductors in wireless power applications," *IEEE Trans. Power Electron.*, vol. 29, no. 1, pp. 481–490, Jan. 2014.
[31] H. L. Krauss and C. W. Bostian, "Resonant circuits and impedance transformation," in *Solid State Radio Engineering*. Hoboken NJ, USA: Wiley, 1980, pp. 76–82.

Babak Noroozi (M'16) received the M.S. degree in biomedical engineering from the Sharif University of Technology, Tehran, Iran, in 1995. He is currently pursuing the Ph.D. degree at the Electrical and Computer Engineering Department, The University of Memphis, Memphis, TN, USA.

His current research interests include wearable wireless passive sensors, embedded systems, and finite-element modeling and analysis.

Bashir I. Morshed (M'12) received the B.Sc. degree in electrical and electronics engineering from the Bangladesh University of Engineering and Technology, Dhaka, Bangladesh, in 2001, the M.Sc. degree in electrical and computer engineering from the University of Windsor, Windsor, ON, Canada, in 2004, and the Ph.D. degree in electrical and computer engineering from Carleton University, Ottawa, ON, in 2010.

Since 2011, he has been an Assistant Professor with the Electrical and Computer Engineering Department, The University of Memphis, Memphis, TN, USA.

Dr. Morshed was a recipient of the Canadian Commonwealth Scholarship in 2002.